Development of a CMUT model for non-linear actuation and contact dynamics

1st Bernard Shieh
Department of Engineering Science
University of Oxford
Oxford, UK
bernard.shieh@eng.ox.ac.uk

2nd Eleanor Stride
Department of Engineering Science
University of Oxford
Oxford, UK
eleanor.stride@eng.ox.ac.uk

***Abstract*—We present a computationally-scalable model for Capacitive Micromachined Ultrasonic Transducer (CMUT) arrays capable of simulating CMUTs in all modes of operation. To solve the fluid-structure problem, a coupled finite element and boundary element method (FE-BEM) is employed. Scalable performance is achieved using data-sparse routines for Hierarchical Matrices. The fluid-structure problem is solved in the frequency domain and used to generate a set of reduced-order linear time-invariant system relating applied mean pressure to mean displacement for a set of lumped sub-domains. A simple non-linear contact model is added to simulate potential contact forces between membrane and substrate. This coupled dynamic system is evolved in time using an algorithm based on fixed-point iteration. The model is validated against finite element software for a representative CMUT geometry and various input voltage signals corresponding to the different regimes of operation.**

***Index Terms*—Transducers, Computational Modeling**

I. Introduction

After an extensive development period, commercial ultrasound probes based on Capacitive Micromachined Ultrasonic Transducers (CMUTs) are beginning to emerge on the market. When compared to the market-leading bulk pieoelectric technology, these probes bring with them a number of disruptive innovations, including improved bandwidth, superior manufacturing flexibility, easier integration with front-end electronics, and reduced costs as a result of batch processing and economies of scales. With the advent of commercially-viable CMUTs there exists a need for practical design and modeling tools appropriate for a rapid development cycle. Growing interest in CMUTs for therapeutic applications [1]–[4] means that these tools should accurately capture CMUT behavior in all regimes of operation, including those involving dynamic collapse of the membranes. However, modeling remains a difficult challenge, involving physical phenomena spanning multiple domains (electrostatic, structural mechanics, acoustics), challenging computational scaling due to coupled acoustic interactions, and actuation forces which are inherently non-linear. We present a model which addresses these challenges. Our multi-domain approach combines several numerical tools together to create a generalizable and scalable model for CMUTs operating in all regimes.

The authors would like to acknowledge funding from the Engineering and Physical Sciences Research Council under Grant No. EP/L024012/1.

II. Methods

A. Solving the fluid-structure problem in the frequency domain

Fluid-structure interactions, which are critical to the frequency behavior of CMUTs in immersion, are modeled using a coupled finite element boundary element method (FE-BEM). For simplicity, linearity is assumed in both the acoustics (valid for small pressure amplitudes) and the structural mechanics (valid for membrane deflections less than the membrane thickness). A fine 2D triangular mesh is generated for each CMUT membrane with each node having a single degree of freedom representing its transverse displacement. The following linear system is assembled at each frequency ω relating the nodal displacements $\vec{u}$ to the nodal forces $\vec{f}$

$$(-\omega^2\mathbf{M} + i\omega\mathbf{C} + \mathbf{K} + i\omega\mathbf{Z}(\omega))\vec{u} = \vec{f} \tag{1}$$

The system matrices are generated in the usual finite element fashion, through the use of shape functions to interpolate the field variables at locations within the elements. For example, the displacement field of an element after transformation $(x, y) \rightarrow (\xi, \eta)$ can be written as a linear combination of the shape functions N_j in the transform coordinates, i.e.

$$u(\xi, \eta) = \sum_{j=1}^{3} u_j N_j \tag{2}$$

$$\mathbf{N} = \begin{bmatrix} \xi \\ \eta \\ 1 - \xi - \eta \end{bmatrix} \tag{3}$$

where u_j are the three nodal displacements associated with the element.

The element mass matrices are generated using a lumped-consistent weighted mass method according to the following expression

$$\mathbf{M}_e = \rho h A_e \left(\mu \iint \mathbf{N}\mathbf{N}^T d\xi d\eta + (1 - \mu)\frac{1}{3}\mathbf{I}_3 \right) \tag{4}$$

where ρ and h are the membrane density and thickness, respectively, A_e is the area of the element, $\mu = 1/2$ for equal weighting, and $\mathbf{I}_3$ is the 3×3 identity matrix.

The element stiffness matrices are generated based on the procedures for *boundary plate triangles* described in [5]. These

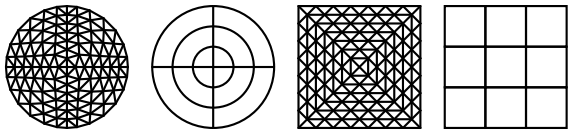

Fig. 1. Example 2D meshes and sub-domain partitioning for circular and square CMUT geometries.

plate elements are rotation-free and are based on classical thin plate theory (Kirchhoff-Love). These elements are accurate so long as the membrane thickness is much less than the smallest longitudinal dimension.

To include the effects of structural damping, a proportional damping model (Rayleigh) is adopted where the global damping matrix is given as a linear combination of the global mass and stiffness matrices, i.e.

$$\mathbf{C} = \alpha\mathbf{M} + \beta\mathbf{K} \tag{5}$$

where α and β are prescribed by the choice of damping ratios at two frequencies.

Finally, the global acoustic impedance matrix $\mathbf{Z}$ is assembled based on a standard boundary element collocation scheme. The pressure at a collocation point $\vec{r}_c$ is given by

$$p(\vec{r}_c) = i\omega\rho_0 \sum_e \sum_{j=1}^{3} \iint \frac{e^{ik|\vec{r}_c - \vec{r}_e|}}{|\vec{r}_c - \vec{r}_e|} N_j(\xi,\eta) A_e d\xi d\eta \tag{6}$$

where ρ_0 is the fluid density, k is the wavespeed, and $\vec{r}_e$ points to the location on the element. The double integral is computed using standard Gauss-Legendre quadrature or modified quadrature rules for cases where the integrand is singular.

Unlike the structural matrices, the acoustic impedance matrix is fully populated due to the global nature of the acoustic interactions. This becomes a source of computational difficulty as the storage and solution of these systems scale with the number of mesh nodes as $O(n^2)$ and $O(n^3)$, respectively. Fortunately, data-sparse techniques have been developed in recent years to address such computational bottle-necks. Namely, hierarchical matrix techniques provide efficient data structures and algorithms for construction, storage, and manipulation of fully-populated matrices using low-rank approximations. We utilize the open-source library H2Lib [6] to implement these techniques.

B. Actuation forces and model order reduction

The membranes are excited into motion from the actuating electrostatic force between the top and bottom electrodes. The electrostatic pressure p_{es} depends non-linearly on the voltage $v(t)$ and transverse deflection according to

$$p_{es} = -\frac{\varepsilon_0}{2} \frac{v(t)^2}{(g + h_{isol}/\varepsilon_r) + u(t)^2} \tag{7}$$

where g is the height of the physical gap between the membrane and the substrate, and h_{isol} is the total thickness of any intervening isolation layers with relative permittivity ε_r.

In addition, contact forces between the membrane and substrate can be considered with a simple non-linear contact model [7].

$$p_{cont} = \frac{3}{2} k\alpha(u(t) + g)\dot{u} - k(u(t) + g); \quad u(t) < -g \tag{8}$$

where α is the coefficient of restitution of the contact pair. Here, the contact is modeled by a linear spring of stiffness k and a damper which scales with penetration.

To consider these forces in an efficient way, it is necessary to reduce the number of degree of freedoms in the model. Rather than consider the forces on each node, the mesh is partitioned into multiple sub-domains wherein the contact forces are assumed to be uniform (see Fig. 1)–an idea first proposed in [8]. For each pair of sub-domains, (1) is solved for uniform loading on one sub-domain and the mean deflection calculated on the other. After inverse Fourier transform, this procedure will produce a set of linear time-invariant (LTI) systems relating mean pressure to mean deflection for every sub-domain pair, i.e. $h_{nm}(t) : \overline{p}_n \rightarrow \overline{u}_m$.

C. An algorithm for solving the time-domain convolution equation

The total mean deflection of each sub-domain is given by

$$\overline{u}_n(t) = \sum_m h_{nm}(t) * \overline{p}_m(t) \tag{9}$$

where $*$ denotes linear convolution. Note that the mean deflection of the sub-domains appear on both the left hand side and right hand side of (9) because the mean pressure can be expanded as the sum of the electrostatic and contact pressures of (7) and (8).

This self-referential expression lends itself naturally to a solution determined using fixed-point iteration. An algorithm was developed based on this approach. Starting at an initial time $t = t_0$ and initial conditions $\overline{u}_n(t_0)$ and $v_n(t_0)$, a *blind* estimate is calculated for the next time step by performing the convolutions of (9) on only the known (solved for) variables for a lag of one time step Δt. Conceptually, this can be understood as evolving the dynamic system to the next time step without consideration of the instantaneous loadings at that step. Written explicitly,

$$\overline{u}_n^{i=0}(T + \Delta t) = \sum_m \left[h_{nm}(t) * \overline{p}_m(t)\right]_{lag=\Delta t}, \quad t \in [t_0, T] \tag{10}$$

where i denotes the iteration number of the estimate, and T denotes the last time for which the variables are known.

The blind estimate can be further refined by considering the estimate as known and applying (9) directly, i.e.

$$\overline{u}_n^{i+1}(T + \Delta t) = \sum_m \left[h_{nm}(t) * \overline{p}_m(t)\right]_{lag=0}, \quad t \in [t_0, T + \Delta t] \tag{11}$$

An important caveat of this approach is that fixed-point iteration may not necessarily converge. More generally, an approximate condition for convergence for an expression $x_{i+1} = f(x_i)$ is given by $|f'(x_0)| < 1$ for the root $x = x_0$.

TABLE I
CMUT MATERIAL PROPERTIES AND GEOMETRY

Material properties	
Density, ρ	2200 $\mathrm{kg/m^3}$
Young's modulus, Y	190 GPa
Poisson's ratio, η	0.28
Relative permittivity, ε_r	7.5
Geometry	
Thickness, h	1 μm
Radius, r_{mem}	30 μm
Gap, g	250 nm
Isolation thickness, h_{isol}	300 nm

As it turns out, the inclusion of contact damping as prescribed in (8) leads to a diverging scheme. To work around this, the iterations are applied first without consideration of the contact damper. The resulting damping pressure is calculated based on this estimate and then assumed to be stationary as the estimate is refined further.

III. Results

Our model was validated against Comsol finite element software (Cambridge, UK) for a representative circular CMUT with material properties and geometry given in Table I. For this comparison, the model was run using eight concentric annular sub-domains. The sampling frequency ranged from 1 GHz to 4 GHz depending on whether contact was expected in the simulation. Contact was modeled in Comsol using a contact pair penalty method. The first and second axi-symmetric resonances were determined by frequency domain analysis to be 3.9 MHz and 15.3 MHz in vacuum, respectively, and 1.4 MHz and 8.2 MHz in water (density = 1000 $\mathrm{kg/m^3}$, sound speed = 1500 $\mathrm{m/s}$).

A. Static and quasi-static operation

Stationary behavior of the CMUT was investigated by gradual application of voltage to set DC voltage levels. The static pull-in voltage $v_{pull-in}$, defined as the maximum DC voltage in which the electrostatic force is sustained by the membrane stiffness, was determined to be 37.2 V by the model and 37.1 V by Comsol. The predicted deflection profiles for voltages below and above are shown in Fig. 2. The maximum error was 3.7% and the mean error 1.1% as percentages of the total gap. This error can be attributed to deviation from classical thin plate theory.

In quasi-static operation (at frequencies significantly below the first resonance), it is expected that the CMUT will behave with a combination of static and dynamic behavior. To demonstrate this case, the CMUT was driven by a 1-cycle 100 kHz 50 V sinusoidal pulse. The mean deflection of the membrane is shown for the central region (Domain 1, $r < r_{mem}/2$) and the outer region (Domain 2, $r > r_{mem}/2$) in Fig. 3. Here, the CMUT is shown to experience dynamic pull-in and release during the positive-going pulse which is repeated when the polarity is reversed. The voltage which these events occur was determined to be 39.5 V for pull-in and 23.4 V for release by the model, as compared with 38.4 V for pull-in and 24.8 V for release by Comsol. The slight time delay observed between the predicted mean displacements just after release can be attributed to this discrepancy.

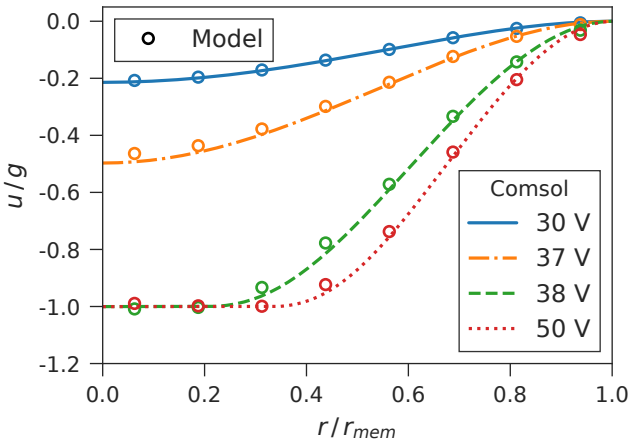

Fig. 2. Static deflection of the CMUT for various DC voltages.

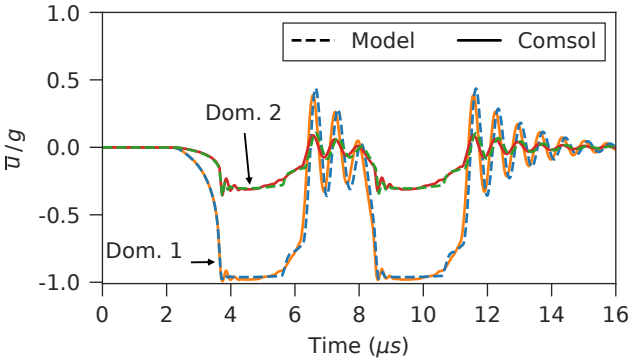

Fig. 3. Mean deflection of the central (Domain 1) and outer (Domain 2) membrane regions for a 1-cycle 100 kHz 50 V sinusoidal pulse.

B. Dynamic operation

Behavior of the CMUT was investigated for dynamic operation with drive signals representing different proposed regimes of operation. In each case, the drive signal consisted of a logistic function DC bias (if applicable) followed by a 40-cycle sinusoidal toneburst. The resulting membrane deflections are plotted as trajectories in the voltage-deflection phase plane which eventually converge to stable orbits representing the predicted steady-state behavior.

To demonstrate standard linear operation, the drive pulse consisted of a 30 V DC bias and a 1 V 1.4 MHz toneburst. As shown in Fig. 4, after a transient response ($t < 10$ μs), the membrane deflection converges to a elliptical orbit characteristic of linear dynamics. In contrast, the CMUT can be driven into a non-linear regime by excitation with a 30 V 0.7 MHz toneburst (no DC bias), representative of a sub-harmonic drive scheme that has been proposed previously [9]. This behavior is also shown in Fig. 4, where a period-halving orbit is observed.

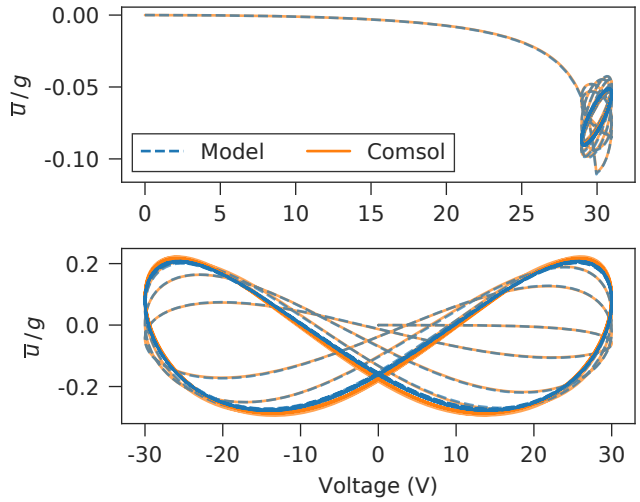

Fig. 4. Phase plane trajectories for a 30 V DC 1 V toneburst (top), and a 0 V DC 30 V toneburst (bottom).

When the voltage of the toneburst is increased to 50 V, 13 V more than the pull-in voltage, the CMUT exhibits repeated collapse and release events, characteristic of so-called *collapse-snapback* operation. It has been suggested that this mode of operation is optimal for the generation of high output pressures due to the large surface velocities generated. To differentiate the behavior of the center of the membrane from the rest of the membrane, the trajectories for both the mean deflection and the maximum deflection are illustrated in Fig. 5a and Fig. 5b.

Finally, *collapse-mode* operation of the CMUT was demonstrated through application of a 60 V DC bias and a 20 V 1.4 MHz toneburst. The trajectories for the mean and maximum deflection are illustrated in Fig. 5c and Fig. 5d. The trajectories indicate that, after the initial collapse event, the membrane remains collapsed for the remainder of the drive signal.

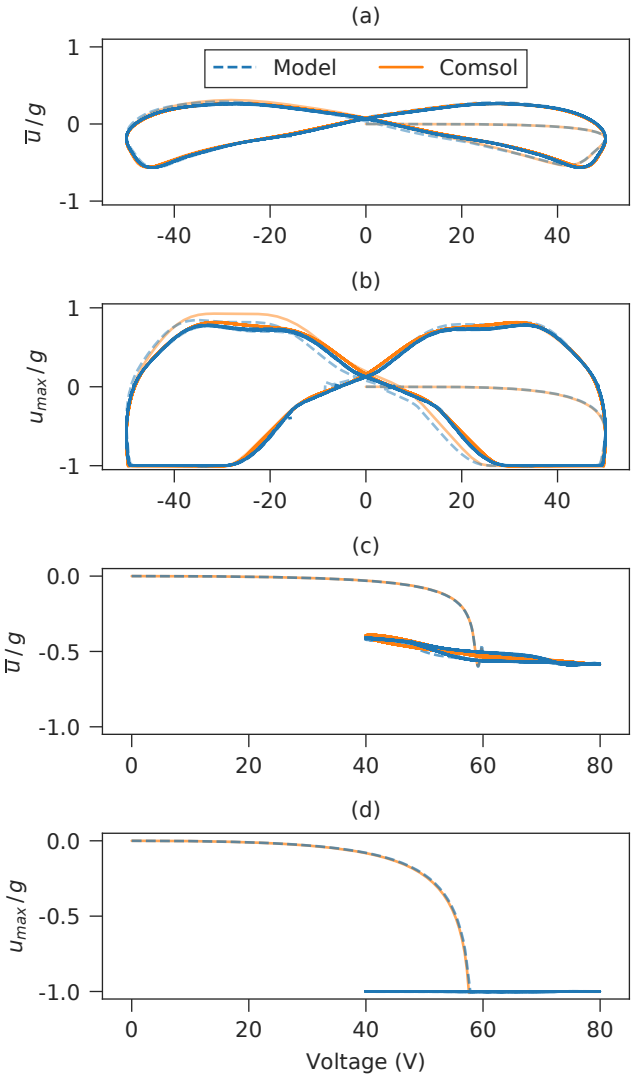

Fig. 5. (a) Mean and (b) maximum deflection trajectories for a 0 V DC 50 V toneburst. (c) Mean and (d) maximum deflection trajectories for a 60 V DC 20 V toneburst.

IV. Conclusion

A scalable and generalizable non-linear model for CMUTs operating in all regimes was presented and validated against finite element software. This model may be useful for the design and optimization of CMUT arrays, especially in therapeutic applications where large output pressures are strongly desired.

References

[1] D. Gross, C. Coutier, M. Legros, A. Bouakaz, and D. Certon, "A cMUT probe for ultrasound-guided focused ultrasound targeted therapy," *IEEE Trans. Ultrason. Ferroelectr. Freq. Control*, vol. 62, pp. 1145–1160, June 2015.

[2] A. Novell, C. B. Arena, O. Oralkan, and P. A. Dayton, "Wideband acoustic activation and detection of droplet vaporization events using a capacitive micromachined ultrasonic transducer," *J. Acoust. Soc. Am.*, vol. 139, p. 3193, June 2016.

[3] H.-S. Yoon, C. Chang, J. H. Jang, A. Bhuyan, J. W. Choe, A. Nikoozadeh, R. D. Watkins, D. N. Stephens, K. Butts Pauly, and B. T. Khuri-Yakub, "Ex vivo HIFU experiments using a 32×32 -element CMUT array," *IEEE Trans. Ultrason. Ferroelectr. Freq. Control*, vol. 63, pp. 2150–2158, Dec. 2016.

[4] C. R. Bawiec, W. A. N'Djin, G. Bouchoux, N. Sénégond, N. Guillen, and J.-Y. Chapelon, "Preliminary investigation of a 64-element capacitive micromachined ultrasound transducer (CMUT) annular array designed for high intensity focused ultrasound (HIFU)," *IRBM*, vol. 39, pp. 295–306, Nov. 2018.

[5] O. Eugenio and F. Zarate, "Rotation-free triangular plate and shell elements," *Int. J. Numer. Methods Eng.*, vol. 47, no. 1-3, pp. 557–603, 2000.

[6] Steffen Borm, "H2lib." http://www.h2lib.org.

[7] D. W. Marhefka and D. E. Orin, "A compliant contact model with nonlinear damping for simulation of robotic systems," *IEEE Transactions on Systems, Man, and Cybernetics - Part A: Systems and Humans*, vol. 29, pp. 566–572, Nov. 1999.

[8] S. Satir, J. Zahorian, and F. L. Degertekin, "A large-signal model for CMUT arrays with arbitrary membrane geometry operating in non-collapsed mode," *IEEE Trans. Ultrason. Ferroelectr. Freq. Control*, vol. 60, pp. 2426–2439, Nov. 2013.

[9] S. Satir and F. L. Degertekin, "Harmonic reduction in capacitive micromachined ultrasonic transducers by gap feedback linearization," *IEEE Trans. Ultrason. Ferroelectr. Freq. Control*, vol. 59, pp. 50–59, Jan. 2012.